

DecepGPT: Schema-Driven Deception Detection with Multicultural Datasets and Robust Multimodal Learning

Jiajian Huang^{1*}, Dongliang Zhu^{2*}, Zitong YU^{1**}, Hui Ma^{1**}, Jiayu Zhang¹, Chunmei Zhu³, and Xiaochun Cao³

¹ Great Bay University

² Wuhan University

³ Sun Yat-sen University

Abstract. Multimodal deception detection aims to identify deceptive behavior by analyzing audiovisual cues for forensics and security. In these high-stakes settings, investigators need verifiable evidence connecting audiovisual cues to final decisions, along with reliable generalization across domains and cultural contexts. However, existing benchmarks provide only binary labels without intermediate reasoning cues. Datasets are also small with limited scenario coverage, leading to shortcut learning. We address these issues through three contributions. First, we construct reasoning datasets by augmenting existing benchmarks with structured cue-level descriptions and reasoning chains, enabling model output auditable reports. Second, we release T4-Deception, a multicultural dataset based on the unified “To Tell The Truth” television format implemented across four countries. With 1695 samples, it is the largest non-laboratory deception detection dataset. Third, we propose two modules for robust learning under small-data conditions. Stabilized Individuality-Commonality Synergy (SICS) refines multimodal representations by synergizing learnable global priors with sample-adaptive residuals, followed by a polarity-aware adjustment that bi-directionally recalibrates representations. Distilled Modality Consistency (DMC) aligns modality-specific predictions with the fused multimodal predictions via knowledge distillation to prevent unimodal shortcut learning. Experiments on three established benchmarks and our novel dataset demonstrate that our method achieves state-of-the-art performance in both in-domain and cross-domain scenarios, while exhibiting superior transferability across diverse cultural contexts. The datasets and codes will be released.

Keywords: Multimodal Deception Detection · Auditable Reasoning · Multicultural Dataset · Stabilized Representation · Modality Consistency

1 Introduction

Multimodal deception detection(MDD) aims to identify deceptive behavior by analyzing audio and visual cues[1], which provide objective decision support in high-stakes social analysis, such as forensic investigation and security screening[2], where human judgment is often subject to cognitive bias[3].

Recent progress in MDD has evolved from handcrafted behavioral descriptors[4] to end-to-end audiovisual deep learning models [5].However, as illustrated in Fig. 1a, traditional MDD method is predominantly label-centric, focusing on optimizing binary classification accuracy. While achieving competitive performance, these method typically provide only a final binary prediction. In forensic and legal contexts, a standalone label is insufficient. Investigators need to understand why a sample is flagged as deceptive, with evidence connecting behavioral cues such as micro-expressions and voice prosody to the final decision. Furthermore, MDD methods must demonstrate generalization across diverse complex cultural contexts to satisfy the requirements of real-world applications[6].

Existing benchmarks[2,7] provide only binary labels without intermediate reasoning cues, preventing models from producing verifiable evidence. Moreover, existing datasets have limited scenario coverage. Important factors, such as identity pretense and cross-cultural variations, are still

* Equal contribution.

** Corresponding authors.

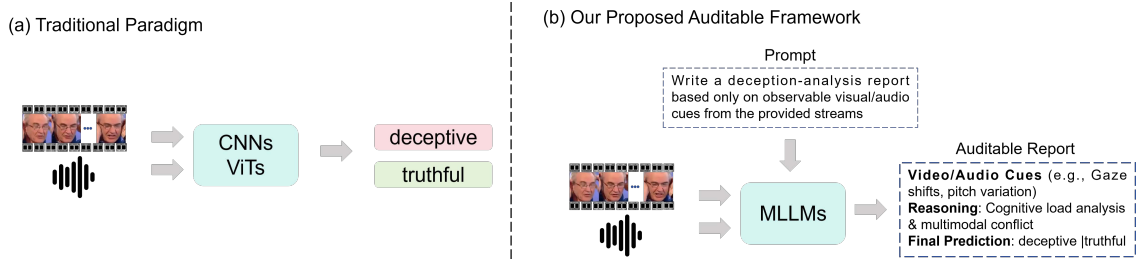


Fig. 1: Comparison between traditional and our auditable method. (a) Traditional methods map behavioral signals directly to binary labels, providing no explanation for the decision. (b) Our method generates structured reports with explicit audiovisual cues and reasoning, creating an audit trail from raw data to final prediction.

not well studied, which limits the generalization ability of MDD methods. In addition, the small scale of available data often causes models to learn spurious correlations[8] during training.

We address these issues through three contributions. First, we construct a reasoning dataset by augmenting existing benchmarks with structured cue-level descriptions and reasoning chains, enabling the generation of auditable reports as shown in Fig. 1b. Second, we release T4-Deception, a multicultural dataset covering identity pretense across four countries (the U.S., Germany, Vietnam, and Bulgaria) under a unified 'To Tell The Truth' television format. With 1695 samples, it is the largest non-laboratory deception benchmark to date. Third, we propose two modules for robust learning under small-data conditions. Stabilized Individuality-Commonality Synergy (SICS) refines multimodal features through a polarity-aware adjustment mechanism, which synergizes a learnable global prior with sample-adaptive residuals to enhance or suppress specific feature dimensions. Meanwhile, Distilled Modality Consistency (DMC) introduces a consistency regularizer that aligns unimodal predictions with multimodal teacher predictions via knowledge distillation to mitigate shortcut learning.

In summary, the main contributions of this article are as follows:

- **Reasoning Dataset.** We provide a standardized pipeline to enrich existing benchmarks with structured audio-visual cues and reasoning chains, enabling the generation of auditable reports for verifiable decision-making.
- **Multicultural Dataset.** We release T4-Deception (To Tell The Truth across 4 cultures), a large-scale dataset covering identity pretense across four countries under a unified television format. With 1695 samples, it is currently the largest non-laboratory dataset in the field.
- **Robust Multimodal Learning Modules.** We propose Stabilized Individuality-Commonality Synergy (SICS) for polarity-aware feature refinement and Distilled Modality Consistency (DMC) for modality consistency distillation, which effectively improve both in-domain and cross-domain performance.

2 Related Work

Multimodal Deception Detection. Early MDD methods relied on handcrafted behavioral cues [4], later evolving into deep end-to-end audiovisual models [9]. Recent benchmarks such as DOLOs highlight the challenges of cross-domain transfer in deception scenarios [2,10]. While Multimodal Large Language Models (MLLMs) [11] offer new potential for semantic reasoning, they struggle to exploit subtle audiovisual cues in deception contexts and are prone to post-hoc hallucinations in rationales [12]. We address this by enforcing a schema-constrained audit report to standardize evidence extraction.

Behavioral Decoupling and Stabilized Refinement. High-stakes deception analysis is often confounded by idiosyncratic identity noise that masks universal deceptive markers [13]. While conventional decomposition [14,15] and modulation paradigms [16] focus on feature separation or sample-dependent weighting, they rarely consider the synergistic stabilization of global priors and individual residuals. Unlike conventional disentanglement, SICS explicitly decouples volatile

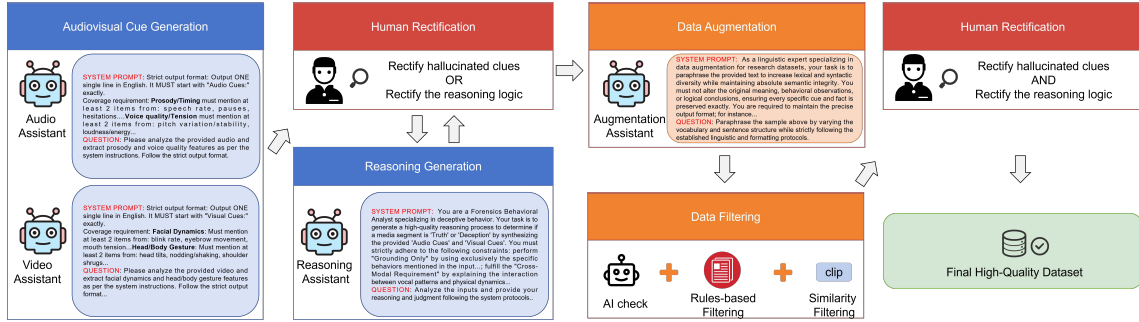


Fig. 2: Overview of reasoning dataset generation pipeline. The pipeline adopts a Human-in-the-Loop (HITL) framework to ensure a high-quality, auditable structured report. It begins with AI-driven audiovisual cue extraction, followed by human-guided rectification of hallucinations. A reasoning assistant then synthesizes these cues into forensic judgments. The data is further enriched through semantic augmentation and a multi-tiered filtering stage (comprising AI, rules-based, and CLIP-similarity checks) to produce the final high-fidelity benchmark.

persona-driven noise from behavioral commonalities to anchor representations in a stabilized latent space for auditable reasoning.

Mitigating Unimodal Dominance. Multimodal optimization often suffers from imbalanced gradients, leading to unimodal shortcuts [17]. Existing methods use modality dropout [18] or adaptive reweighting [19]. In contrast, we regularize *prediction distributions* via cross-modal consistency constraints. This reduces shortcut reliance while maintaining full inference efficiency.

3 Method

To provide the transparency required for sensitive decision-making, we propose an auditable paradigm. As illustrated in Fig. 2, this paradigm is realized through a standardization pipeline that enriches existing benchmarks with the fine-grained behavioral descriptions and reasoning logic necessary for structured reporting. To address the performance instability inherent in small-data regimes and the lack of cross-cultural benchmarks designed under a unified scenario protocol, we construct and release a dataset (Table 1 and Fig. 3) that increases total data volume while filling critical gaps in identity pretense and multicultural scenarios. In parallel, we introduce two robust encoding modules (Fig. 4) to further stabilize optimization: Stabilized Individuality-Commonality Synergy (SICS), which enhances representation robustness by suppressing noise, and Distilled Modality Consistency (DMC), which prevents unimodal shortcuts through consistency distillation. Together, these components ensure that the generated audit reports are grounded in balanced and verifiable auditable evidence.

3.1 Data Construction: Structured Multi-Cue Reasoning Supervision

Schema Design. We use a structured output format: [Audio Cues; Visual Cues; Reasoning; Prediction]. The model first identifies deception-related audio and visual cues, then performs cross-modal reasoning based on these cues to derive the final prediction. This enforces an evidence-to-conclusion inference flow, where the prediction is derived from explicit behavioral observations through intermediate reasoning steps.

HITL Generation Pipeline. As shown in Fig. 2, our pipeline uses multiple specialized assistants. The Audio Assistant (Qwen-Omni) extracts audio cues such as prosody and speech patterns. The Video Assistant (GPT-4o) extracts visual cues, including facial dynamics and body language. A Reasoning Assistant (GPT-4o) then synthesizes these cues into a cross-modal judgment. Human annotators review the outputs from these three assistants to correct hallucinations or logical inconsistencies. An Augmentation Assistant (GPT-4o) then paraphrases the text to increase lexical variation. The augmented samples pass through automated filters before a final human review.

Multi-stage Filtering. After the data augmentation process, we apply three rigorous filtering stages to the augmented samples. First, AI-based checks automatically remove contradictory cue-reasoning pairs to ensure logical consistency. Second, rule-based filtering strictly ensures full format

Table 1: Comparison of multimodal deception detection datasets. T4-Deception (To Tell The Truth across 4 cultures) dataset is the largest non-laboratory benchmark, featuring a unified identity pretense task across multiple cultural contexts.

Dataset	Total	Deceptive	Truthful	Setting	Deceptive Task
Real Life Trials [1]	121	61	60	Courtroom	False Testimony
Bag of Lies [7]	325	162	163	Laboratory	False Image-Narration
MU3D [20]	320	160	160	Laboratory	False Social-Evaluation
Deception Det. [21]	1680	630	1050	Laboratory	False Interview-Anecdotes
Box of Lies [22]	1049	862	187	Game Show	False Object-Description
DOLOs [2]	1675	899	776	Game Show	False Story-Telling
T4-Deception (Ours)	1695	1130	565	Game Show	False Professional-Identity
— <i>U.S. Edition</i>	876	584	292	Game Show	(Unified Multi-Culture)
— <i>German Edition</i>	702	468	234	Game Show	
— <i>Vietnam Edition</i>	66	44	22	Game Show	
— <i>Bulgarian Edition</i>	51	34	17	Game Show	

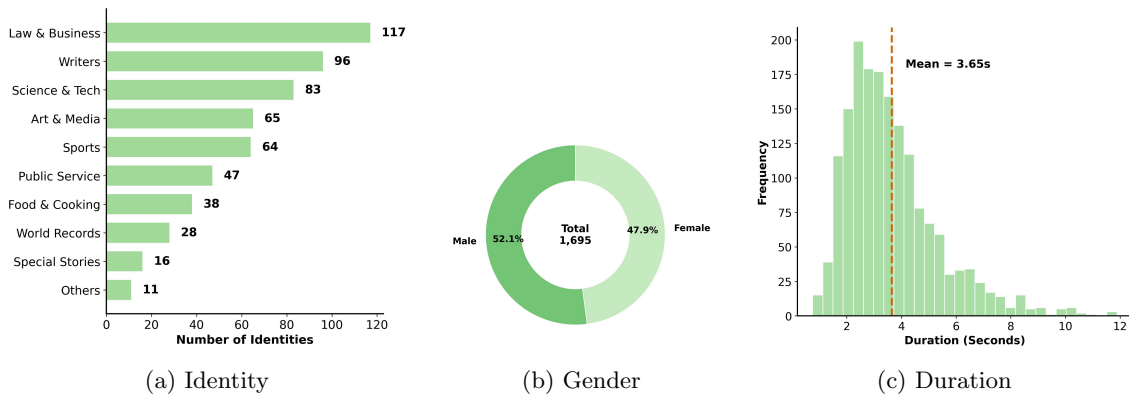


Fig. 3: Dataset statistics of T4-Deception. We illustrate: (a) distribution of identities, where each one of the total 565 identities is shared by one truthful and two deceptive participants; (b) balanced gender distribution; and (c) numerous short-term deceptive segments with an average temporal duration of 3.65s.

compliance across all entries. Third, similarity filtering effectively prevents data redundancy by eliminating near-duplicate samples. Finally, the filtered samples undergo a comprehensive final human review to confirm overall data quality and reliability.

3.2 T4-Deception (To Tell The Truth across 4 cultures) Dataset

To address data scarcity in deception detection, we present the T4-Deception (To Tell The Truth across 4 cultures) dataset, the largest non-laboratory benchmark for multimodal deception detection. Prior datasets are limited to a single cultural background, as data collection was restricted to one geographic or linguistic region per task. In contrast, T4-Deception covers a consistent high-stakes scenario—identity pretense—across diverse populations from the United States, Germany, Vietnam, and Bulgaria.

As detailed in Table 1, our dataset distinguishes itself from prior work on deceptive tasks and cross-cultural contexts. While existing game-show datasets primarily focus on object fabrication (e.g., Box of Lies[22]) or story fabrication (e.g., DOLOs [2]), T4-Deception necessitates that subjects maintain a fully fabricated persona—encompassing professional skills and personal backgrounds—throughout intense interpersonal confrontations. This rigorous setting elicits complex visual and acoustic behavioral markers, such as subtle facial dynamics reflecting emotional shifts. Comprising 1,695 samples from four countries, the dataset facilitates a robust analysis of

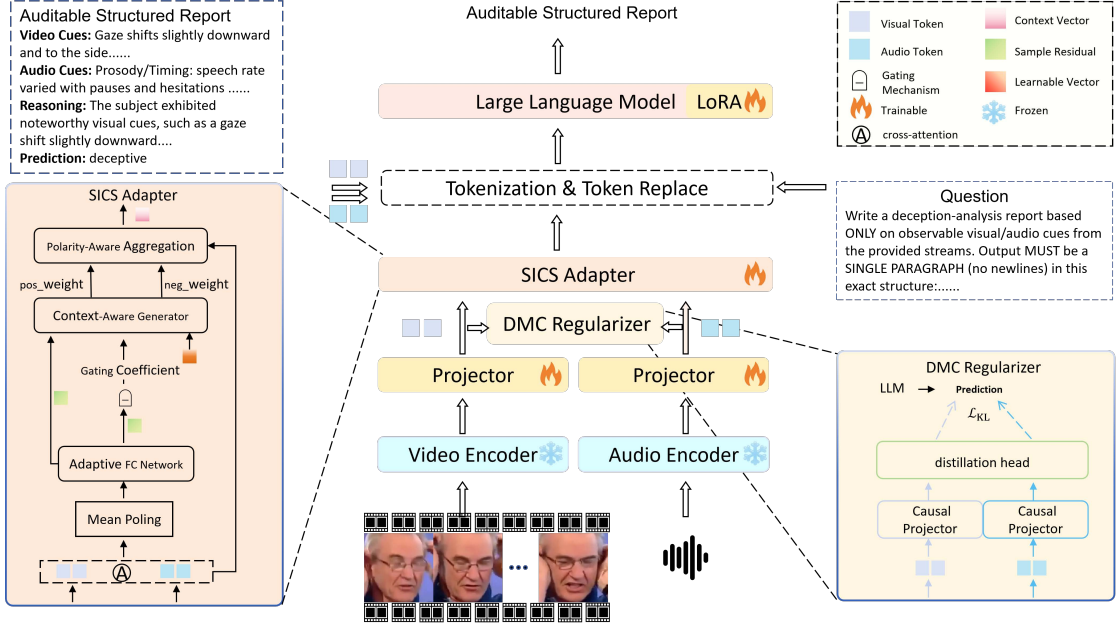


Fig. 4: Overview of our auditable audiovisual deception detection framework. A video encoder and an audio encoder extract modality features, followed by a fusion module that produces a robust representation. Inside the encoder/fusion stage, we integrate two mechanisms: (1) **Stabilized Individuality-Commonality Synergy (SICS)** that combines a shared baseline with a sample-specific residual via gated fusion (with a light stability regularizer); (2) **Distilled Modality Consistency (DMC)** that discourages unimodal dominance by penalizing high-confidence cross-modal conflict through agreement regularization on modality-specific predictive distributions. A report generator then produces a *single-line, schema-constrained* report (**Video Cues**; **Audio Cues**; **Reasoning**; **Prediction**), which serves as a standardized audit artifact.

behavioral variance across cultural contexts. Furthermore, as illustrated in Fig. 3, T4-Deception exhibits high diversity in professional identities. With an average duration of 3.65s and a maximum of 11.89s, these concise segments enable models to concentrate on immediate deceptive cues and micro-expression transitions critical to interpersonal confrontation.

3.3 Stabilized Individuality-Commonality Synergy (SICS)

The SICS adapter refines input features through polarity-aware adjustment (visualized in the left of Fig. 4). It generates sample-adaptive weights by fusing a learnable global vector with context-derived residuals. Two independent transformations then produce positive and negative adjustment coefficients to enhance or suppress feature dimensions. The adjusted features are combined with the original input via a residual connection. The details are described below:

Given an input feature $x_i \in \mathbb{R}^{L \times d}$, the module first calculates the temporal mean to obtain a context vector $c_i \in \mathbb{R}^d$, which is then processed by a two-layer fully connected network to generate the sample-adaptive residual $\Delta z_i \in \mathbb{R}^d$:

$$c_i = \frac{1}{L} \sum_{j=1}^L x_{i,j}, \quad \Delta z_i = \mathbf{W}_2(\tanh(\mathbf{W}_1 c_i + b_1)) + b_2, \quad (1)$$

where L denotes the sequence length, and \mathbf{W}, b are learnable weights and biases.

Subsequently, a gating coefficient g_i is computed to determine the fusion ratio between a learnable global vector $b_{global} \in \mathbb{R}^d$ and the generated residual Δz_i :

$$g_i = \sigma(\mathbf{W}_g \Delta z_i + b_g), \quad w_i = \tanh(g_i \cdot b_{global} + (1 - g_i) \cdot \Delta z_i). \quad (2)$$

The module then applies two learnable transformations to produce positive and negative adjustment weights:

$$w_i^+ = \mathbf{W}^+ w_i + b^+, \quad w_i^- = \mathbf{W}^- w_i + b^-, \quad (3)$$

where \mathbf{W}^+ , \mathbf{W}^- , b^+ , and b^- are independent learnable parameters. The input features are refined as:

$$x'_i = x_i \odot \text{ReLU}(w_i^+) - x_i \odot \text{ReLU}(w_i^-), \quad (4)$$

where \odot denotes element-wise multiplication. Finally, the output is calculated as a weighted sum of the refined features and the original input:

$$\text{Output}_i = \lambda \cdot x'_i + (1 - \lambda) \cdot x_i, \quad (5)$$

where λ is a balancing hyperparameter and we empirically set $\lambda = 0.2$.

3.4 Distilled Modality Consistency (DMC)

To mitigate unimodal shortcut learning, we introduce the DMC regularizer (visualized in the bottom-right inset of Fig. 4), which encourages visual and audio modalities to produce consistent predictions during training.

As shown in Fig. 4, the DMC module consists of modality-specific causal projectors followed by a shared distillation head. These components map the frozen visual and audio tokens to the label space $\mathcal{Y} = \{\text{deceptive}, \text{truthful}\}$. Specifically, the unimodal prediction p_m is generated as:

$$p_m(y) = \text{softmax}(\Phi_{\text{distill}}(\text{Proj}_m(h_m)))(y), \quad m \in \{v, a\}, y \in \mathcal{Y}, \quad (6)$$

where h_m represents the modality tokens, Proj_m is the Causal Projector, and Φ_{distill} denotes the distillation head.

The MLLM decoder produces a teacher distribution $q(y)$ at the final **Prediction** position when conditioning on the full multimodal context and the schema constraint. We minimize the KL divergence between the unimodal predictions from the shared distillation head and this MLLM decoder teacher:

$$\mathcal{L}_{\text{distill}} = \sum_{m \in \{v, a\}} \text{KL}(q \| p_m). \quad (7)$$

DMC regularizer encourages both modality projection heads to function effectively, which is discarded during inference.

3.5 Auditable Report Generation with Schema Constraint

We generate the auditable report directly with an MLLM. Given video V_i and audio A_i , the MLLM encoder produces modality-specific hidden states and a fused audiovisual representation:

$$H_{v,i}, H_{a,i}, H_{va,i} = \text{Enc}_{\text{MLLM}}(V_i, A_i), \quad (8)$$

where $H_{v,i}$ and $H_{a,i}$ capture modality-specific feature for visual and acoustic signals, respectively. $H_{va,i}$ captures the cross-modal interactions between them.

Conditioned on these representations, the MLLM decoder then generates a structured, single-line schema-constrained report that provides the essential behavioral evidence required for a comprehensive and auditable deception analysis:

$$R_i = \text{Dec}_{\text{MLLM}}(H_{v,i}, H_{a,i}, H_{va,i}; \text{schema}). \quad (9)$$

The schema enforces a fixed field order and semicolon delimiters: **Video Cues**; **Audio Cues**; **Reasoning**; **Prediction**. We supervise the MLLM to match the target report text, and require the final **Prediction** field to match the ground-truth label (**deceptive/truthful**).

3.6 Training Objective

We jointly optimize the schema-constrained report generation task alongside regularizers. The overall objective function is defined as:

$$\mathcal{L} = \mathcal{L}_{\text{rep}} + \alpha \mathcal{L}_{\text{distill}}, \quad (10)$$

where \mathcal{L}_{rep} denotes the token-level cross-entropy loss for generating the structured audit report. The term $\mathcal{L}_{\text{distill}}$ represents the consistency distillation loss derived from our DMC module. We empirically set $\alpha = 0.1$ to balance the accuracy of the generated reports and the mitigation of unimodality reliance.

4 Experiments

We evaluate our method on six aspects: (i) in-domain effectiveness across diverse deceptive tasks, (ii) cross-domain generalization under dataset shift, (iii) cross-cultural robustness in identity pretense, (iv) component contributions via ablation studies, (v) visualization analysis of SICS adapter and DMC regularizer, (vi) reasoning capability analysis. Core code, reasoning samples, and T4-Deception subsets are in the supplement; full release follows acceptance.

4.1 Implementation Details

We build on AffectGPT [23], an emotion-centric MLLM integrating Qwen-7B, Whisper-large-v2 [24], and CLIP-ViT-L/14 [25], with projectors pre-trained on the MER2023 emotion dataset [26]. During fine-tuning, the encoders remain frozen; we apply LoRA to the LLM while fully training the projectors and our proposed components. Optimization is performed for 200 epochs using AdamW ($LR = 5 \times 10^{-5}$). Training is conducted on a single NVIDIA H100 (80GB) with a batch size of 4, sampling 8 frames per video at 224×224 resolution.

4.2 Datasets and Protocols

To verify the effectiveness of our method, we evaluate our model on three established benchmarks and our newly introduced dataset, T4-Deception:

- **Bag-of-Lies (BoL)** [7]: 325 lab-collected samples on false image-narration.
- **MU3D** [20]: 320 lab-collected samples on false social-evaluation.
- **DOLOs** [2]: 1,675 game show samples on false story-telling.
- **T4-Deception (Ours)**: 1695 samples across four cultural contexts: U.S. (876), Germany (760), Vietnam (66), and Bulgaria (51), collected under a unified false professional-identity task.

For the established benchmarks, we conduct in-domain evaluations following official protocols (3-fold for BoL and DOLOs; 4-fold for MU3D), alongside cross-domain assessments. We also perform in-cultural evaluations via 3-fold cross-validation and pairwise cross-cultural tests.

4.3 MLLM Configuration

We compare our method against two types of MLLMs:

Commercial MLLMs (Zero-shot). Commercial models, including GPT-4o [27] and so on, are evaluated via API calls in a zero-shot setting due to limited parameter access. These represent the reasoning capabilities of general-purpose models without task-specific training.

Open-source MLLMs (Fine-tuned). We fine-tune representative open-source MLLMs, including Qwen3-Omni [28], VideoLLaMA2 [29] and so on. These models are trained using LoRA on the same training sets as our method.

Unified Prompting and Output Schema. All models use the same schema-constrained prompt format. Models output a single-line structured record: **Video Cues; Audio Cues; Reasoning; Prediction.**

Table 2: Comprehensive In-domain Benchmark. We evaluate performance across three datasets: DOLOs, Bag-of-Lies (BoL), and MU3D. **Set.:** ZS=Zero-shot, LoRA=Fine-tuning, Full=Full Training. **Mod.:** A=Audio, V=Video, AV=Audio-Visual.

Method/Model	Source	Set.	Mod.	DOLOs		BoL		MU3D	
				Acc.	F1	Acc.	F1	Acc.	F1
<i>Task-specific Deep Learning Methods</i>									
LieNet [30]	TCDS'22	Full	AV	56.50	69.72	59.78	58.14	53.48	33.62
FacialCueNet [5]	AI'23	Full	V	60.98	68.65	56.23	63.26	57.64	59.13
PECL [2]	ICCV'23	Full	AV	64.75	71.20	59.51	51.06	55.31	60.07
AFFAKT [31]	AAAI'25	Full	AV	68.10	70.73	–	–	–	–
<i>Large Multimodal Models (LMMs)</i>									
GPT-4o [27]	Comm.	ZS	V	66.38	64.21	57.14	56.35	54.12	52.47
Qwen-Omni [28]	Comm.	ZS	AV	51.72	49.56	45.27	35.82	50.23	41.38
VideoLLaMA2 [29]	Open	LoRA	AV	53.48	56.12	47.65	49.34	51.84	54.62
SALMONN2 [32]	Open	LoRA	AV	52.63	55.44	46.82	48.51	51.06	53.79
Qwen2.5-7B-VL [28]	Open	LoRA	AV	46.10	52.37	44.24	41.15	53.86	56.24
DecepGPT	ours	LoRA	AV	73.23	76.13	63.46	63.72	61.25	67.22

Table 3: Cross-Domain Evaluation on DOLOs (D), Bag-of-Lies (B), and MU3D (M). “X&Y→Z” denotes training on X and Y, testing on Z.

Method	M&B → D		D&M → B		D&B → M		Average	
	Acc.	F1	ACC	F1	Acc.	F1	Acc.	F1
LieNet [30]	54.40	68.23	54.69	50.51	51.08	59.75	53.39	59.50
PECL [2]	54.51	69.55	51.25	66.95	55.38	52.46	53.71	62.99
Ours	63.46	61.79	59.62	72.00	57.24	60.38	60.11	64.72

4.4 In-Domain Evaluation

As shown in Table 2, our method achieves state-of-the-art performance across all three benchmarks. First, compared to zero-shot commercial giants (e.g., GPT-4o [27]), our method yields consistent accuracy gains of +6.85% on DOLOs, +6.32% on BoL, and +7.13% on MU3D. Second, compared to fine-tuned open-source MLLMs (e.g., VideoLLaMA2 [29]), our method yields consistent accuracy gains of +19.75% on DOLOs, +15.81% on BoL, and +7.39% on MU3D. Finally, our approach even surpasses specialized task-specific models (e.g., PECL [2], AFFAKT [31]) by margins of +5.13% (DOLOs), +3.68% (BoL), and +3.61% (MU3D). These results are achieved via efficient LoRA fine-tuning while generating structured audit reports, offering both higher accuracy and better interpretability than baselines that output simple labels.

4.5 Cross-Domain Evaluation

We evaluate the generalization ability of our method under dataset shift by training on source datasets and directly testing on target domains without target-domain fine-tuning. Table 3 demonstrates that our method consistently outperforms task-specific methods (e.g., PECL) on all transfer paths in accuracy: +8.95% (M&B → D), +4.93% (D&M → B), and +1.86% (D&B → M), with a +6.40% average gain. Regarding F1 score, our method also achieves improvements: +5.05% (D&M → B) and +0.63% (D&B → M), with a +1.73% average gain.

4.6 Evaluation on T4-Deception

We conduct a comprehensive evaluation on the T4-Deception dataset, including both **in-cultural** and **cross-cultural** assessments across four distinct regions: U.S., Germany, Vietnam, and Bulgaria. As shown in Table 4, we train models on each source culture and evaluate them on all four targets (including the source itself) in a zero-shot manner. In-cultural Performance: When trained and tested on the same culture (diagonal entries), our method achieves stable baseline performance,

Table 4: Comprehensive Evaluation on T4-Deception. We report Accuracy (Acc) and F1 Score for both in-cultural (diagonal, **bold**) and cross-cultural (off-diagonal) settings. Models are trained on the row culture and tested on the column culture.

Train ↓ / Test →	U.S.		Germany		Vietnam		Bulgaria	
	Acc	F1	Acc	F1	Acc	F1	Acc	F1
U.S.	64.65	73.28	59.50	52.14	57.58	61.20	63.00	71.62
Germany	57.00	57.26	61.11	53.33	56.06	59.14	60.78	62.45
Vietnam	55.48	61.05	54.87	48.92	63.10	68.42	58.82	64.10
Bulgaria	58.19	63.38	56.45	50.18	54.55	58.76	61.46	66.25

Table 5: Main ablation study across three datasets. Base refers to the model without the SICS adapter and DMC regularization.

Variant	DOLOs		Bag-of-Lies		MU3D	
	Acc.	F1	Acc.	F1	Acc.	F1
Base (no SICS/DMC)	67.24	71.18	57.69	54.26	53.75	65.34
Base + DMC	68.77	71.94	59.62	58.15	55.00	66.27
Base + SICS	72.68	76.02	62.50	61.43	60.15	67.08
Full (SICS + DMC)	73.23	76.13	63.46	63.72	61.25	67.22

with an average accuracy of 62.58% (e.g., 64.65% for U.S. and 61.11% for Germany). This confirms the model’s ability to capture culture-specific deception markers effectively. More importantly, the model demonstrates strong generalization capabilities when transferred to unseen cultures (off-diagonal entries). For instance, the model trained on the U.S. region retains 59.50% accuracy when tested on Germany, showing only a marginal drop compared to the in-domain setting. Across all 12 cross-cultural transfer pairs, the average performance remains stable at 57.69%, with an average relative degradation of only 4.89% compared to in-cultural results. Further comparative analysis of cross-cultural deception is provided in Appendix A.

4.7 Ablation Study

Main Ablation Study. We evaluate the contribution of each core component across **all three datasets**, as detailed in Table 5. Both SICS and DMC consistently improve over the baseline, though their impact varies by dataset. On DOLOs, SICS provides a significant accuracy gain of +5.44%, while DMC adds a further +1.53%. Similarly, on Bag-of-Lies, SICS boosts accuracy by +4.81%, with DMC contributing an additional +1.93%. For MU3D, we observe a substantial improvement of +6.40% from SICS and +1.25% from DMC. The full model, combining both modules, achieves the best performance across all benchmarks, yielding an average accuracy gain of +6.42% over the baseline. These results confirm that SICS and DMC address complementary aspects of robust multimodal learning. The cross-domain transfer performance of these ablated variants is provided in Appendix B.

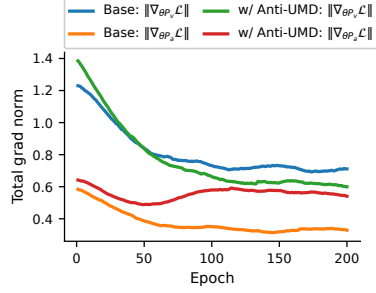
Component Analysis and Backbone Comparison. To further validate the effectiveness of the internal mechanisms, we conduct detailed ablation studies on the SICS adapter components and compare different backbone networks. Due to space limitations, we report the results on the **DOLOs** dataset here as a representative example; the complete results for Bag-of-Lies and MU3D are detailed in Appendix C. As shown in Table 6, removing any component of the SICS adapter (global prior, polarity-aware adjustment, or gating mechanism) leads to a clear drop in performance, confirming their necessity. Furthermore, we investigate the impact of the backbone architecture (Table 7). Replacing the LLM backbone with simpler structures (MLP or Transformer) results in significantly lower performance. This suggests that the LLM backbone provides superior semantic reasoning capabilities essential for this task.

Table 6: Ablation on SICS components.

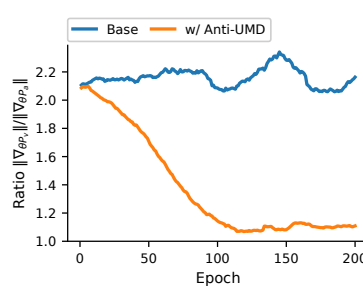
Variant	Acc.	F1
w/o b_{global}	71.42	74.31
w/o Polarity	72.06	75.28
w/o Gating	71.85	74.94
Full SICS	73.23	76.13

Table 7: Comparison of backbones.

Backbone	Acc.	F1
MLP[33]	58.42	60.17
Transformer[34]	64.75	68.34
Ours (LLM)	73.23	76.13



(a) Gradient on Projector

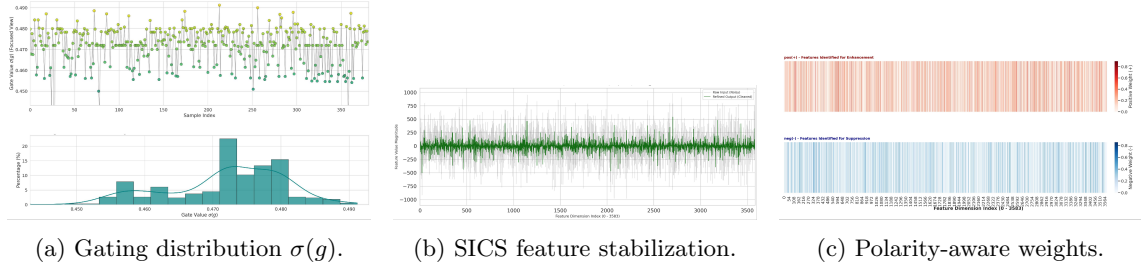


(b) Gradient Ratio on Projector

Fig. 5: Projector gradient dynamics analysis during training.

5 Visualization and Interpretability Analysis

We analyze the internal mechanisms of the SICS Adapter and DMC Regularizer from two aspects: (i) unimodal shortcut mitigation in the DMC Regularizer, and (ii) representation stabilization in the SICS Adapter; We also assess the fidelity of the generated auditable evidence, verifying that it is grounded in the extracted behavioral cues to provide a transparent audit trail for the final prediction.

(a) Gating distribution $\sigma(g)$.

(b) SICS feature stabilization.

(c) Polarity-aware weights.

Fig. 6: Visualization analysis of the SICS Adapter. (a) Dynamic variation of gating values on the fusion of global priors and local residuals. (b) Comparison between volatile raw features and stabilized features processed by SICS. (c) Adjustment where positive weights enhance informative feature and negative weights suppress noise feature.

5.1 Visualization Analysis of the DMC Regularizer

Fig. 5 illustrates how the DMC Regularizer affects cross-modal feature utilization. Fig. 5a tracks the gradient norms backpropagated to the modality-specific projectors. In the base setting, the visual projector receives larger gradients, indicating a bias toward visual cues. With the DMC Regularizer, visual-side gradients are initially higher as the consistency constraint activates, followed by gradual strengthening of acoustic-side gradients. This suggests that the DMC Regularizer helps the model incorporate audio evidence. Fig. 5b shows the dynamics via the ratio $r = \|\nabla_{\theta_{P_v}}\|/\|\nabla_{\theta_{P_a}}\|$. The base model shows visual dominance ($r > 1$), while the DMC Regularizer reduces this ratio closer to unity. These results indicate that the DMC Regularizer helps balance gradient flow across modalities, supporting more balanced multimodal learning.

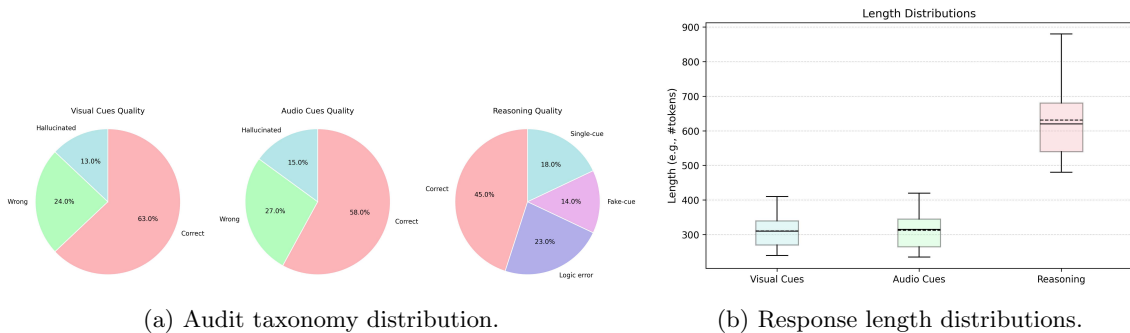


Fig. 7: Quantitative audit analysis. (a) distribution of cue correctness and reasoning quality categories; (b) text length distribution of reasoning.

5.2 Visualization Analysis of the SICS Adapter

We visualize the adaptive gating distribution, the denoising effect, and the polarity-aware weights to illustrate the SICS Adapter as shown in Fig. 6.

Dynamic gating behavior. Fig. 6a shows the gating coefficient $\sigma(g)$ varies across samples (mostly within $[0.443, 0.493]$). This indicates that the fusion is not a static offset but adapts to each sample. This supports the individuality–commonality synergy: the adapter maintains stable features for typical cases while allowing flexibility to model persona-specific residuals for outliers.

Feature stabilization and noise suppression. In small-data regimes, audiovisual learning can be affected by high-magnitude persona-driven noise (e.g., individual behaviors or recording conditions). Fig. 6b compares feature magnitudes before and after SICS Adapter: raw features show spiky, volatile dimensions, while refined features are smoother and more centered. This suggests that the SICS Adapter reduces such variations, improving numerical stability.

Polarity-aware enhancement vs. suppression. Fig. 6c visualize the learned positive (enhancement) and negative (suppression) weights. The adjustment from polarity-aware may help produce more discriminative features for the MLLM.

5.3 Auditable Reasoning: Validity and Case Study

We use structured, schema-constrained reports (**Cues**; **Reasoning**; **Prediction**) as audit artifacts to identify hallucinations and shortcut rationales. We audit these reports along two axes with an error taxonomy: (i) Visual/Acoustic Cues, categorized as Correct, Counterfactual, or Non-existent (hallucinated); (ii) Reasoning Quality, classified as Correct, False-cue (logical but counterfactual), Incoherent, or Single-cue (modal collapse).

Quantitative distributions and answer length statistics (Fig. 7) demonstrate that our framework significantly enhances behavioral understanding. Qualitative analysis in Fig. 8 further contrasts success and failure cases, highlighting how the generated schema-constrained reasoning chains explicitly reveal the evidentiary basis for each prediction. These artifacts collectively enable post-hoc human verification of model logic without requiring access to internal black-box states.

6 Conclusion

We present an auditable framework for multimodal deception detection, transitioning from opaque binary classification to structured evidentiary reasoning. Our pipeline enriches existing benchmarks with multimodal cues and reasoning data. To address data scarcity and cultural bias, we introduce T4-Deception, the largest non-laboratory dataset comprising 1,695 samples across four cultural contexts. Furthermore, the SICS Adapter and DMC Regularizer are proposed to stabilize representations and suppress shortcut learning in small-data regimes. Experiments demonstrate that our approach achieves state-of-the-art performance while providing verifiable evidence for high-stakes behavioral analysis.

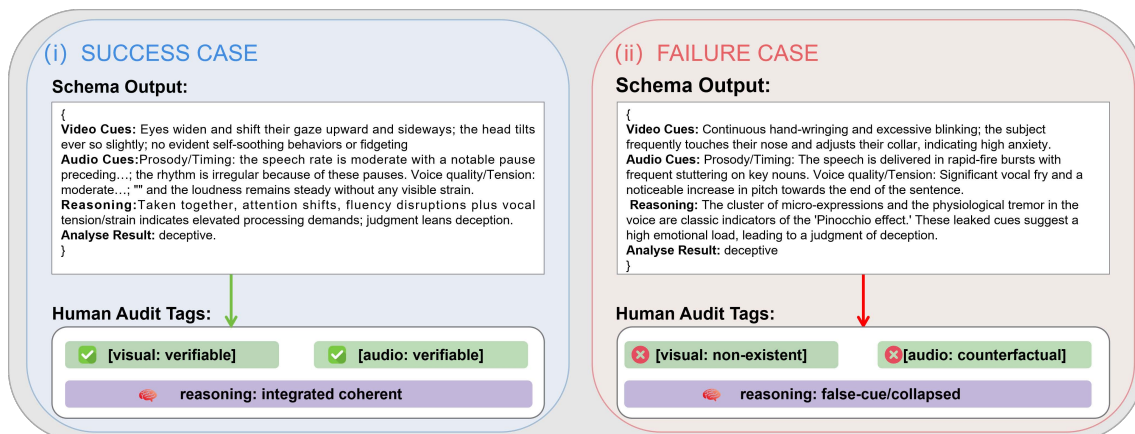


Fig. 8: Qualitative comparison of a success case vs. a failure case with human audit tags.

References

- Verónica Pérez-Rosas, Mohamed Abouelenien, Rada Mihalcea, and Mihai Burzo. Deception detection using real-life trial data. In *Proceedings of the 2015 ACM on international conference on multimodal interaction*, pages 59–66, 2015.
- Xiaobao Guo, Nithish Muthuchamy Selvaraj, Zitong Yu, Adams Wai-Kin Kong, Bingquan Shen, and Alex Kot. Audio-visual deception detection: Dolos dataset and parameter-efficient crossmodal learning. In *Proceedings of the IEEE/CVF International Conference on Computer Vision*, pages 22135–22145, 2023.
- Charles F Bond Jr and Bella M DePaulo. Accuracy of deception judgments. *Personality and social psychology Review*, 10(3):214–234, 2006.
- Verónica Pérez-Rosas, Mohamed Abouelenien, Rada Mihalcea, Yao Xiao, CJ Linton, and Mihai Burzo. Verbal and nonverbal clues for real-life deception detection. In *Proceedings of the 2015 conference on empirical methods in natural language processing*, pages 2336–2346, 2015.
- Borum Nam, Joo Young Kim, Beomjun Bark, Yeongmyeong Kim, Jiyeon Kim, Soon Won So, Hyung Youn Choi, and In Young Kim. Facialcuenet: unmasking deception-an interpretable model for criminal interrogation using facial expressions: Iy kim et al. *Applied Intelligence*, 53(22):27413–27427, 2023.
- Verónica Pérez-Rosas and Rada Mihalcea. Cross-cultural deception detection. In *Proceedings of the 52nd Annual Meeting of the Association for Computational Linguistics (Volume 2: Short Papers)*, pages 440–445, 2014.
- Viresh Gupta, Mohit Agarwal, Manik Arora, Tanmoy Chakraborty, Richa Singh, and Mayank Vatsa. Bag-of-lies: A multimodal dataset for deception detection. In *Proceedings of the IEEE/CVF conference on computer vision and pattern recognition workshops*, pages 1–8, 2019.
- Robert Geirhos, Jörn-Henrik Jacobsen, Claudio Michaelis, Richard Zemel, Wieland Brendel, Matthias Bethge, and Felix A Wichmann. Shortcut learning in deep neural networks. *Nature Machine Intelligence*, 2(11):665–673.
- Zhe Wu, Bharat Singh, Larry Davis, and V Subrahmanian. Deception detection in videos. In *Proceedings of the AAAI conference on artificial intelligence*, volume 32, 2018.
- Xiaobao Guo, Zitong Yu, Nithish Muthuchamy Selvaraj, Bingquan Shen, Adams Wai-Kin Kong, and Alex C Kot. Benchmarking cross-domain audio-visual deception detection. *arXiv preprint arXiv:2405.06995*, 2024.
- Haotian Liu, Chunyuan Li, Qingyang Wu, and Yong Jae Lee. Visual instruction tuning. volume 36, pages 34892–34916, 2023.
- Md Messal Monem Miah, Adrita Anika, Xi Shi, and Ruihong Huang. Hidden in plain sight: Evaluation of the deception detection capabilities of llms in multimodal settings. In *Proceedings of the 63rd Annual Meeting of the Association for Computational Linguistics (Volume 1: Long Papers)*, pages 31013–31034, 2025.
- Devamanyu Hazarika, Roger Zimmermann, and Soujanya Poria. Misa: Modality-invariant and-specific representations for multimodal sentiment analysis. In *Proceedings of the 28th ACM international conference on multimedia*, pages 1122–1131, 2020.
- Konstantinos Bousmalis, George Trigeorgis, Nathan Silberman, Dilip Krishnan, and Dumitru Erhan. Domain separation networks. *Advances in neural information processing systems*, 29, 2016.

15. Zemin Tang, Qi Xiao, Xu Zhou, Yangfan Li, Cen Chen, and Kenli Li. Learning discriminative multi-representation representations for multimodal sentiment analysis. *Information Sciences*, 641:119125, 2023.
16. John Arevalo, Thamar Solorio, Manuel Montes-y Gómez, and Fabio A González. Gated multimodal units for information fusion. *arXiv preprint arXiv:1702.01992*, 2017.
17. Xiaokang Peng, Yake Wei, Andong Deng, Dong Wang, and Di Hu. Balanced multimodal learning via on-the-fly gradient modulation. In *Proceedings of the IEEE/CVF conference on computer vision and pattern recognition*, pages 8238–8247, 2022.
18. Natalia Neverova, Christian Wolf, Graham Taylor, and Florian Nebout. Moddrop: adaptive multimodal gesture recognition. *IEEE Transactions on Pattern Analysis and Machine Intelligence*, 38(8):1692–1706, 2015.
19. Chengxiang Huang, Yake Wei, Zequn Yang, and Di Hu. Adaptive unimodal regulation for balanced multimodal information acquisition. In *Proceedings of the Computer Vision and Pattern Recognition Conference*, pages 25854–25863, 2025.
20. E Paige Lloyd, Jason C Deska, Kurt Hugenberg, Allen R McConnell, Brandon T Humphrey, and Jonathan W Kunstman. Miami university deception detection database. *Behavior research methods*, 51(1):429–439, 2019.
21. Jeremy Speth, Nathan Vance, Adam Czajka, Kevin W Bowyer, Diane Wright, and Patrick Flynn. Deception detection and remote physiological monitoring: A dataset and baseline experimental results. In *2021 IEEE International Joint Conference on Biometrics*, pages 1–8, 2021.
22. Felix Soldner, Verónica Pérez-Rosas, and Rada Mihalcea. Box of lies: Multimodal deception detection in dialogues. In *Proceedings of the 2019 Conference of the North American Chapter of the Association for Computational Linguistics: Human Language Technologies, Volume 1 (Long and Short Papers)*, pages 1768–1777, 2019.
23. Zheng Lian, Haiyang Sun, Licai Sun, Jiangyan Yi, Bin Liu, and Jianhua Tao. Affectgpt: Dataset and framework for explainable multimodal emotion recognition. *arXiv preprint arXiv:2407.07653*, 2024.
24. Alec Radford, Jong Wook Kim, Tao Xu, Greg Brockman, Christine McLeavey, and Ilya Sutskever. Robust speech recognition via large-scale weak supervision. In *International conference on machine learning*, pages 28492–28518, 2023.
25. Alec Radford, Jong Wook Kim, Chris Hallacy, Aditya Ramesh, Gabriel Goh, Sandhini Agarwal, Girish Sastry, Amanda Askell, Pamela Mishkin, Jack Clark, et al. Learning transferable visual models from natural language supervision. In *International conference on machine learning*, pages 8748–8763, 2021.
26. Zheng Lian, Haiyang Sun, Licai Sun, Zhuofan Wen, Siyuan Zhang, Shun Chen, Hao Gu, Jinming Zhao, Ziyang Ma, Xie Chen, et al. Mer 2024: Semi-supervised learning, noise robustness, and open-vocabulary multimodal emotion recognition. In *Proceedings of the 2nd International Workshop on Multimodal and Responsible Affective Computing*, pages 41–48, 2024.
27. Aaron Hurst, Adam Lerer, Adam P Goucher, Adam Perelman, Aditya Ramesh, Aidan Clark, AJ Ostrow, Akila Welihinda, Alan Hayes, Alec Radford, et al. Gpt-4o system card. *arXiv preprint arXiv:2410.21276*, 2024.
28. Jin Xu, Zhifang Guo, Hangrui Hu, Yunfei Chu, Xiong Wang, Jinzheng He, Yuxuan Wang, Xian Shi, Ting He, Xinfu Zhu, et al. Qwen3-omni technical report. *arXiv preprint arXiv:2509.17765*, 2025.
29. Zesen Cheng, Sicong Leng, Hang Zhang, Yifei Xin, Xin Li, Guanzheng Chen, Yongxin Zhu, Wenqi Zhang, Ziyang Luo, Deli Zhao, et al. Videollama 2: Advancing spatial-temporal modeling and audio understanding in video-llms. *arXiv preprint arXiv:2406.07476*, 2024.
30. Mohan Karnati, Ayan Seal, Anis Yazidi, and Ondrej Krejcar. Lienet: a deep convolution neural network framework for detecting deception. *IEEE transactions on cognitive and developmental systems*, 14(3):971–984, 2021.
31. Zihan Ji, Xuetao Tian, and Ye Liu. Affakt: A hierarchical optimal transport based method for affective facial knowledge transfer in video deception detection. In *Proceedings of the AAAI Conference on Artificial Intelligence*, volume 39, pages 1336–1344, 2025.
32. Changli Tang, Yixuan Li, Yudong Yang, Jimin Zhuang, Guangzhi Sun, Wei Li, Zejun Ma, and Chao Zhang. video-salmonn 2: Caption-enhanced audio-visual large language models. *arXiv preprint arXiv:2506.15220*, 2025.
33. Ilya O Tolstikhin, Neil Houlsby, Alexander Kolesnikov, Lucas Beyer, Xiaohua Zhai, Thomas Unterthiner, Jessica Yung, Andreas Steiner, Daniel Keysers, Jakob Uszkoreit, et al. Mlp-mixer: An all-mlp architecture for vision. *Advances in neural information processing systems*, 34:24261–24272, 2021.
34. Ashish Vaswani, Noam Shazeer, Niki Parmar, Jakob Uszkoreit, Llion Jones, Aidan N Gomez, Łukasz Kaiser, and Illia Polosukhin. Attention is all you need. *Advances in neural information processing systems*, 30, 2017.

Appendix

A Comprehensive Analysis of T4-Deception

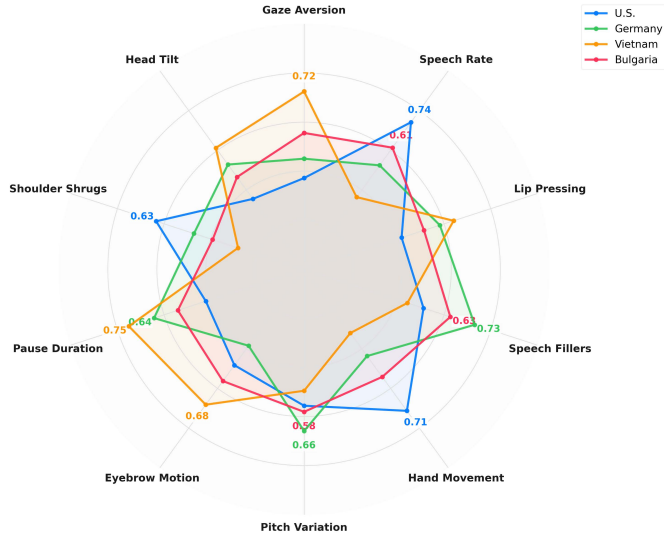


Fig. A1: Cross-cultural distribution of deceptive signatures across 10 behavioral dimensions.

This appendix provides a comprehensive analysis of the **T4-Deception** dataset ($N = 1,695$) in three aspects:

Cross-Cultural Behavioral Dynamics: We quantify cross-cultural variations in deceptive cues and examine how these patterns drive dynamic modality reliance in our model (Section A.1).

Subject Diversity: With 1,695 strictly independent subjects, our dataset far exceeds the scale of existing *non-laboratory* datasets (typically ~ 213 subjects), thereby providing a significantly richer variety of samples (Section A.2).

Baseline Evaluation: We evaluate the classic deception detection methods on our dataset, establishing a baseline for future research (Section A.3).

A.1 Cross-Cultural Behavioral Dynamics

We quantify deceptive cues through ten visual and acoustic features: Gaze Aversion, Speech Rate, Lip Pressing, Speech Fillers, Hand Movement, Pitch Variation, Eyebrow Motion, Pause Duration, Shoulder Shrugs, Head Tilt.

Cue Distribution Figure A1 visualizes the different cultural behavioral patterns: the U.S. subjects exhibit higher *Hand Movement* intensity, whereas the Vietnamese subjects show pronounced *Pause Duration*.

Dynamic Modality Reliance Since deception cues vary by culture, DecepGPT automatically adjusts which signals it trusts most. As shown in Figure A2, the model relies primarily on **video** (62.4%) for **U.S.** subjects. In contrast, for **Vietnamese** subjects, it shifts focus to **audio** (68.2%), where speech pauses serve as key indicators. Meanwhile, for subjects from **Germany and Bulgaria**, the model adopts a **balanced mix** of both video and audio cues.

A.2 Subject Diversity

As illustrated in Figure A3, T4-Deception features a significantly larger pool of unique subjects compared to existing deception detection datasets.

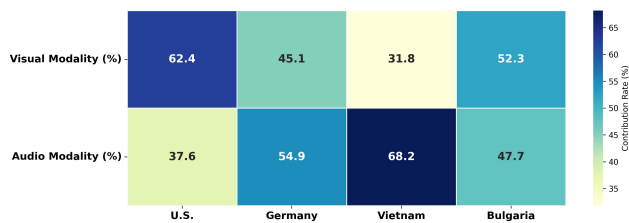


Fig. A2: Cross-cultural modality contribution rates. The model dynamically shifts reliance between visual and audio streams.

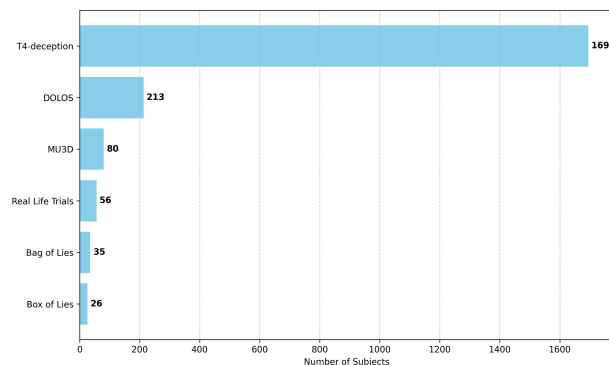


Fig. A3: Comparison of Unique Subject Counts Across Deception Datasets.

A.3 Baseline Evaluation

We evaluate DecepGPT against task-specific baselines as shown in Table A1.

Table A1: Comparison with task-specific baselines in T4-deception on accuracy.

Method	U.S.	Germany	Vietnam	Bulgaria	Avg.
LieNet	52.41	50.85	48.23	51.16	50.66
FacialCueNet	54.12	52.60	49.54	53.08	52.3
PECL	56.45	54.12	51.76	55.42	54.44
DecepGPT	64.65	61.11	63.10	61.46	62.58

B Cross-Domain Ablation Study of SICS and DMC

Table B1 details how SICS or DMC affects the model’s ability to generalize across different datasets, while the main text focuses on in-domain evaluation.

C Detailed Component Analysis and Backbone Comparison

We provide the comprehensive component analysis and backbone comparison results for the Bag-of-Lies and MU3D datasets as shown in Table C.1 and Table C.2, complementing the DOLOS results shown in the main text.

C.1 Fine-Grained Ablation of SICS Components

Table C1 confirms that removing any SICS component (global prior, polarity-aware adjustment, or gating) consistently degrades performance across both datasets, validating the necessity of each module.

C.2 Backbone Architecture Comparison

Table C2 shows that the LLM backbone significantly outperforms MLP and Transformer alternatives on Bag-of-Lies and MU3D, highlighting the critical role of advanced semantic reasoning in multimodal deception detection.

Table B1: Cross-domain ablation study on core modules. “X&Y→Z” denotes training on datasets X and Y, testing on the held-out target Z.

Variant	M&B → D		D&M → B		D&B → M		Average	
	Acc.	F1	Acc.	F1	Acc.	F1	Acc.	F1
Base (No SICS/DMC)	54.12	58.20	50.50	64.50	51.20	54.30	51.94	59.00
Base + DMC	56.45	59.88	53.21	66.75	52.84	56.12	54.17	60.92
Base + SICS	61.08	60.43	57.44	69.82	55.60	59.15	58.04	62.13
Full Model	63.46	61.79	59.62	72.00	57.24	60.38	60.11	64.72

Table C1: Ablation study on SICS internal components across standard benchmarks.

Variant	DOLOs		Bag-of-Lies		MU3D	
	Acc.	F1	Acc.	F1	Acc.	F1
w/o b_{global}	71.42	74.31	61.22	61.05	58.85	64.12
w/o Polarity	72.06	75.28	60.20	59.40	59.40	65.25
w/o Gating	71.85	74.94	61.85	61.32	59.10	65.50
Full SICS	73.23	76.13	63.46	63.72	61.25	67.22

D Linguistic Quality of Reasoning Chains

Beyond classification accuracy, we rigorously evaluate the quality of the generated auditable reports. This section first defines the evaluation metrics used, followed by the comparative results.

D.1 Evaluation Metrics

To comprehensively assess the generated reasoning chains, we employ a hybrid evaluation strategy combining standard NLP metrics and LLM-based scoring:

- **METEOR**: Measures semantic alignment via exact word matches, stems, synonyms, effectively evaluating fluency, adequacy of forensic descriptions.
- **ROUGE-L**: Evaluates longest subsequences between generated reports and ground-truth annotations, focusing on sentence structural similarity.
- **BERTScore**: Computes token-level cosine similarity using contextual BERT embeddings. This captures deep semantic equivalence despite surface differences, ensuring reasoning aligns with expert analysis.
- **GPT-Score (LLM-as-a-Judge)**: We use GPT-4o to score *logical coherence*, *evidence grounding*, and *clarity* (1–10). This overcomes n-gram metric limitations in evaluating complex reasoning quality.

Table C2: Comparison of backbone architectures on standard benchmarks. The LLM-based approach significantly outperforms traditional deep learning backbones.

Backbone	DOLOs		Bag-of-Lies		MU3D	
	Acc.	F1	Acc.	F1	Acc.	F1
MLP	58.42	60.17	51.25	48.90	52.10	56.45
Transformer	64.75	68.34	56.84	55.42	55.62	61.08
DecepGPT	73.23	76.13	63.46	63.72	61.25	67.22

D.2 Comparative Results

As shown in Table D1, DecepGPT achieves superior performance across all metrics compared to general-purpose MLLMs. The high BERTScore (0.812) and GPT-Score (6.96) indicate that our schema-driven approach effectively grounds the reasoning in forensic evidence rather than generating generic hallucinations.

Table D1: Linguistic evaluation of generated reasoning reports. Higher scores indicate better quality.

Method	METEOR	ROUGE-L	BERTScore	GPT-Score
GPT-4o (Zero-shot)	0.284	0.312	0.765	5.42
VideoLLaMA2 (LoRA)	0.215	0.246	0.792	5.15
Qwen2.5-7B-VL (LoRA)	0.242	0.285	0.804	5.28
DecepGPT	0.342	0.384	0.812	6.96